Available online at www.sciencedirect.com
ScienceDirect
Physica C 456 (2007) 144–152
PHYSICA C
www.elsevier.com/locate/physc

Review

Neutron irradiation effects on two gaps in MgB_2

V. Ferrando [a,*], M. Affronte [b], D. Daghero [c], R. Di Capua [d], C. Tarantini [a], M. Putti [a]

[a] CNR-INFM-LAMIA and Dipartimento di Fisica, University of Genova, Via Dodecaneso 33, 16146 Genova, Italy
[b] CNR-INFM-S3 and Dipartimento di Fisica, University of Modena e Reggio Emilia, Via G. Campi 213/A, I-41100 Modena, Italy
[c] Dipartimento di Fisica and CNISM, Politecnico di Torino, 10129 Torino, Italy
[d] University of Napoli and CNR/INFM-Coherentia, Via Cinthia, 80126 Napoli, Italy

Received 18 January 2007; received in revised form 24 January 2007; accepted 25 January 2007
Available online 6 February 2007

Abstract

In this paper, an overview of the gaps behaviour as a function of disorder in neutron-irradiated samples is presented. The general effects of neutron irradiation is discussed and, by comparing the different experiments performed in literature, we show that this technique is very effective to introduce disorder in a controlled way in MgB_2. Then, the three experiments that allowed determining the two gaps, i.e. specific heat, point contact spectroscopy and scanning tunnelling spectroscopy measurements are analysed and compared, and the role of interband scattering is discussed.

Keywords: Magnesium diboride; Neutron irradiation; Two-gap behavior

Contents

1. Introduction

The superconductivity in the binary compound MgB_2 [1] is characterized by the presence of two gaps related to different sheets of the Fermi surface. This compound represents, up to now, the only system in which this feature has been clearly observed, although two-gap superconductivity had been theoretically studied since the 1950s [2,3]. The Fermi level is crossed by two kinds of partially filled energy bands, from which superconductivity takes place: two σ bands, originated by p_{xy} B orbitals, and two π bands, originated by p_z B orbitals. The two gaps are associated to these bands; the π gap, Δ_π, has a value of about 2 meV, while the σ gap, Δ_σ, is about 7 meV.

* Corresponding author. Tel.: +39 0103536323.
E-mail address: ferrandov@ge.infm.it (V. Ferrando).

0921-4534/$ - see front matter © 2007 Published by Elsevier B.V.
doi:10.1016/j.physc.2007.01.016

The multiband feature of MgB_2 is at the origin of very peculiar behaviors concerning the effects of scattering, both intraband and interband. In particular, interband scattering by non-magnetic impurities causes pair breaking, as magnetic impurities do in conventional superconductors, therefore suppressing the critical temperature down to the value of the equivalent BCS system with isotropic coupling. In addition, in the strong interband scattering limit, a complete isotropization of the Fermi surface is expected to occur and the two gaps should merge into a BCS gap. This topic was already studied before the discovery of MgB_2 [4], and of course it has been recently revisited for the specific case [5,6]. The value of critical temperature corresponding to the merging of the gaps has been calculated from first principles to be in the range 19–26 K [7–9].

Many experimental efforts have been made to confirm this effect, introducing disorder by chemical substitution or irradiation, but no saturation of the critical temperature has been observed.

The suppression of superconductivity can be due to several mechanisms (among which the σ-band filling is the most effective, especially in doped MgB_2), while the merging of the gaps can be induced only by the interband scattering. Therefore only a direct observation of the crossover from two- to single-gap regime can provide the final evidence for the validity of two-band model [10].

It is widely accepted that the Δ_π value is poorly affected by disorder while Δ_σ exhibits a linear decrease, at least in the T_c range from optimal samples to about 25 K. This has been observed in Al-substituted [11–13], C-substituted [14–17], neutron irradiated [18,19] samples as well as in disordered films [20]. On the other hand, in samples with lower critical temperature the results are contradictory, both about the merging T_c and the scaling of gaps. Only in one series of C-doped single crystals the merging of the gaps has been observed when T_c was suppressed down to 19 K [16].

The main problem in the experiments performed on MgB_2 disordered samples is the poor control on the effects induced on a dirty sample having such a complex physics. In particular, chemical substitutions may induce several effects related to charge doping, structural instability and inhomogeneous distribution of impurities. Moreover, if the reference, nominally clean, samples are not optimal, further uncertainty degree is added, which is often the case of thin films. So far, neutron irradiation seems to be one of the best ways to overcome these problems because it does not induce remarkable changes in the band structure, providing a homogeneous defect distribution. In this paper, an overview of the effects of neutron irradiation on the two gaps, verified by various experimental techniques and on different kind of samples, will be presented. After a brief description of the neutron irradiation process, point contact spectroscopy (PCS) and specific heat measurements on polycrystalline samples and scanning tunnelling spectroscopy (STS) experiments on thin films will be described and finally, the results will be discussed and compared.

2. Neutron irradiation effects on MgB_2

In neutron irradiation experiments, both fast and thermal neutrons play a role. The energy of fast neutrons is high enough to induce point defects by direct collisions with nuclei. Thermal neutrons instead have low energy, but can anyway produce disorder in magnesium diboride through the neutron capture reaction of the ^{10}B nuclei. As a consequence of this process, the ^{10}B nuclei decay in a 0.84 MeV ^7Li nucleus and in an alpha particle, whose energy depends on the final state of lithium (1.7 MeV or 1.47 MeV if the decay is in the fundamental state (7% of the cases) or in the first excited state, respectively). It is at the end of the recoil (4.8 and 2.1 μm, respectively) that the two emitted particles, losing their energy, produce defects and displacements. In MgB_2, this capture reaction has such a large cross section that the damage could be highly inhomogeneous. For example, in a standard MgB_2 bulk sample, usually made by natural Boron where the ^{10}B content is about 20%, the neutron penetration depth would be about 200 μm, resulting in a non uniform defect distribution throughout the sample. This problem has been overcome in different ways.

Apart from the pioneering work of Ref. [21], where the critical temperature of a bulk sample was reduced down to 5 K irradiating at high fluence, the effects of neutron irradiation were extensively discussed in Ref. [22], where the authors suggested the use of a cadmium foil in order to absorb thermal neutrons. Polycrystalline samples [22] and single crystals grown at ETH in Zurich [23] were irradiated in the TRIGA MARK reactor in Wien. The same procedure has been applied in the work of Ref. [18], who investigated the properties of neutron irradiated polycrystalline bulk samples by specific heat measurements, as it will be discussed in the following.

Another approach, proposed to ensure a uniform defect distribution also in massive samples, was to prepare MgB_2 with isotopically enriched ^{11}B, where the ^{10}B, responsible for the neutron capture reaction, is only 0.5% [24,25]. Here, the starting samples were irradiated at the spallation neutron source SINQ of Paul Scherrer Institut (PSI) in Villigen. A complete series of homogeneous disordered samples was obtained, with T_c down to 9 K and extremely narrow transitions. This set of samples was used to carry out several experiments in order to observe the influence of disorder on the properties of magnesium diboride [19,25,26].

The last route proposed to avoid self-shielding is to irradiate samples made with natural boron but with size smaller than the neutron penetration depth, i.e. thin films [27] or wires [28]. In Ref. [27], extremely clean thin films grown by hybrid physical chemical vapor deposition (HPCVD) were irradiated at PSI at different neutron fluences, until superconductivity is completely suppressed.

Finally, in the experiment by Wilke et al. [28], the samples were thin wires with a diameter of about 140 μm with T_c close to the bulk value, irradiated at Missouri University

Research Reactor. The critical temperature was suddenly reduced to 5 K already in the less damaged sample, due to the higher content of ^{10}B.

The upper panel of Fig. 1 reports T_c as a function of neutron fluence for four experiments made on Cd shielded bulk samples [18] and single crystals [23], polycrystals made with ^{11}B [25] and thin films [27] is plotted. The critical temperature progressively decreases down to few Kelvin and all the four series of data fall almost on the same curve, showing that, in this range of neutron fluence, the different approaches are equivalent to produce a systematic increase of disorder in MgB_2. This result is confirmed also by the resistivity dependence on fluence reported in the lower panel [18,25,27]. Here the data for single crystals were not available, but the agreement of the other three series is surprisingly good: by increasing the neutron fluence up to 10^{20} cm^{-2}, the residual resistivity increases by two orders of magnitude with the same trend.

To summarize the effect of neutron irradiation on MgB_2, Fig. 2 shows the behaviour of critical temperature as a function of resistivity again for bulks [18,25] and films [27]. It is worth noticing that no sign of the saturation is present close to 19–26 K, differently from what predicted by the two-band model [7–9]. On the contrary, the same linear decrease can be observed for the three experiments, with T_c vanishing at about 100 μΩ cm. All these data evidence that neutron irradiation is a reliable technique to introduce defects in magnesium diboride without changing the charge of the system and lead to very well reproducible series of samples to study fundamental properties as a function of disorder.

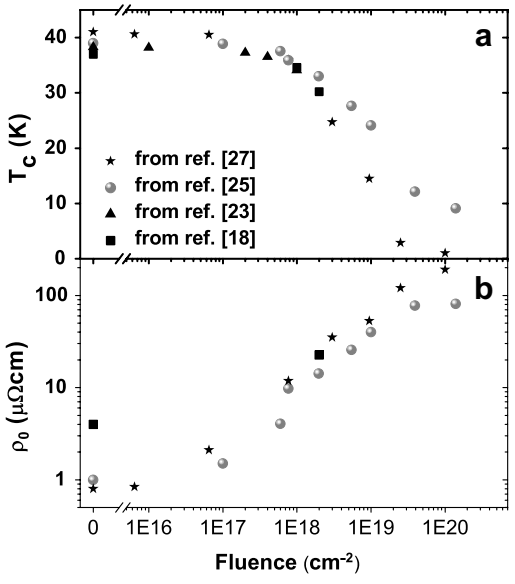

Fig. 1. Critical temperature (a) and residual resistivity at 42 K (b) as a function of neutron fluence for thin films [27], polycrystalline samples made with ^{11}B [25] and shielded with Cd [18] and single crystals with Cd shield [23].

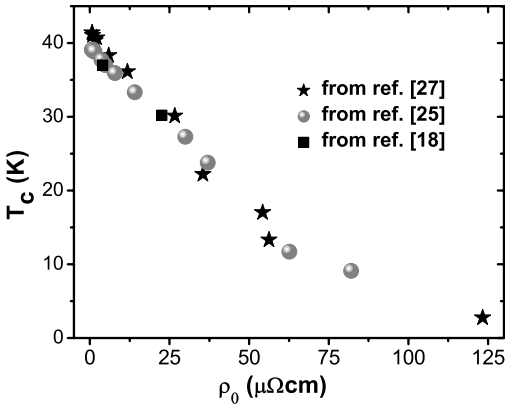

Fig. 2. Critical temperature as a function of residual resistivity for films [27] and polycrystals made with ^{11}B from Ref. [25] and shielded with cadmium [18].

3. Sample description

The samples that will be considered in the following are both thin films and bulk samples, irradiated at the spallation neutron source SINQ at PSI in Villigen where thermal and fast neutron flux densities are 1.6×10^{13} cm^{-2} s^{-1} and 10^{10} cm^{-2} s^{-1}, respectively.

Polycrystalline bulk samples were prepared with isotopically pure ^{11}B at the University of Genova following the procedure reported in [29], which gives high quality samples with no spurious phases, low resistivity (1–2 μΩ cm) and optimum T_c about 39 K. The samples were cut in parallelepiped bars and irradiated at different fluences up to 1.4×10^{20} cm^{-2}. Table 1 summarizes the characteristics of the bulk samples: T_c decreases down to 9 K and residual resistivity increases by more than two orders of magnitude. The transition width, estimated by susceptibility measurements, remains extremely small (about 0.5 K) even in the most exposed sample P6, indicating that the defects distribution is highly homogeneous; it is worth noticing that similar ΔT_c values were obtained also by specific heat measurements [19].

The films (epitaxial, 2000 Å thick) were grown by HPCVD at The Pennsylvania State University [30], nominally in the same conditions, and then exposed to neutron fluences from 6.4×10^{15} to 9.5×10^{18} cm^{-2}. Each film was

Table 1
Main properties of the irradiated bulks

Sample	Neutron fluence (cm^{-2})	T_c (K)	ΔT_c (K)	ρ_0 (μΩ cm)
P0	0	38.8	0.3	0.8
P3	7.6×10^{17}	35.6	0.2	7.8
P3.5	2×10^{18}	32.6	0.5	14
P3.7	5.5×10^{18}	25.8	0.6	30
P4	1×10^{19}	20.7	0.9	38
P5	3.9×10^{19}	11.0	0.4	63
P6	1.4×10^{20}	8.7	0.5	82

T_c and ΔT_c, determined by susceptibility measurements, are defined as $T_{c50\%}$ and as $T_{c90\%}$–$T_{c10\%}$, respectively. The resistivity values were corrected by $\rho_{corr} = \rho\Delta\rho_{teo}/\Delta\rho_{sper}$ [31].

Table 2
Main properties of the measured irradiated films

Sample	Neutron fluence (cm^{-2})	T_c (K)	ΔT_c (K)	ρ_0 ($\mu\Omega$ cm)
IRR10	6.4×10^{15}	41.0	0.1	0.9
IRR30	7.7×10^{17}	36.1	0.4	12
IRR35	3.0×10^{18}	22.2	2.3	36
IRR40	9.5×10^{18}	14.5	4	55

T_c and ΔT_c, determined by resistive measurements, are defined as $T_{c50\%}$ and as $T_{c90\%}$–$T_{c10\%}$, respectively.

sealed under vacuum in a small quartz ampoule just after deposition; this setup allowed to perform irradiation also for long times without compromising samples quality. The properties of the films are summarized in Table 2: the critical temperature ranges from 41 to 14.5 K and residual resistivity increases by almost two orders of magnitude. The transition width is small in less irradiated samples (less than 0.5 K) and increases in IRR40 but, as shown in Ref. [27] it decreases again at higher irradiation level, being of the order of 0.2 K in the most heavily irradiated sample. A similar behavior trend is present also in irradiated bulks (see Table 1).

The samples reported in Tables 1 and 2 are part of those plotted in Figs. 1 and 2 (Refs. [25,27], respectively).

4. Gap determination in bulk samples

4.1. Specific heat

Specific heat is a technique that provides information on the bulk properties not influenced by fluctuation or surface effects. On the other hand it probes all the bulk material and it is sensitive to the presence of spurious phases or inhomogeneities. In order to extract reliable information on the energy gaps it is necessary to deal with pure and homogeneous samples: in this sense, irradiated samples are a good choice.

The specific heat of MgB_2 was analyzed [32] within a generalized α-model which linearly superposes the contributions from two σ and π bands. In this case, a BCS temperature dependence of the superconducting gaps is assumed, and the amplitude of the reduced gaps at $T=0$ K, $\alpha_\sigma=\Delta_\sigma(0)/k_BT_c$, $\alpha_\pi=\Delta_\pi(0)/k_BT_c$, are introduced as adjustable parameters. The σ and π bands contribute to the superconducting specific heat proportionally to the γ_σ/γ and γ_π/γ fractions, where γ is the Sommerfeld's coefficient and γ_σ and γ_π are the σ and π contribution to it. This model was successfully applied to pure MgB_2, where the interband scattering is small, but it is not *a priori* applicable to a strongly disordered sample. However the two-gap model was compared with full solution of the two-band Eliashberg theory [9]. In spite of the strong modifications of the density of states by interband scattering, the two-gap α-model is sufficiently accurate to extract gap values from the specific heat also in the case of disordered samples. Therefore, specific heat data on irradiated samples can be reliably analyzed within this model.

The first experiment of specific heat on irradiated MgB_2 was performed by Wang et al. [18]. In this experiment a polycrystalline sample shielded with a cadmium foil was irradiated in two different steps to a fast neutron fluence of 10^{18} and $2\times10^{18}\,cm^{-2}$ and the critical temperature was reduced down to about 30 K. The specific heat was measured before and after each irradiation in the temperature range 2–50 K and in order to estimate the normal state specific heat a magnetic field of 14 T was applied.

In the second experiment [19], the specific heat was measured in the samples P0, P3.5, P3.7, P4, P5 and P6 described in the previous section. The specific heat was measured in the temperature range 2–40 K in an applied magnetic field of 0 and 7 T.

The electronic specific heat c_{sc} can be calculated once the phonon contribution has been subtracted: $c_{sc}=c(H=0)-[\beta T^3+\delta T^5]$; the phonon contribution is estimated by fitting the normal-state specific heat in magnetic field with the curve $c(H=7\text{ T})=\gamma T+\beta T^3+\delta T^5$.

$c_{sc}/\gamma T$ for the samples P0, P4, P5, P6 are reported in Fig. 3. The evidence of the π-gap comes by the excess of

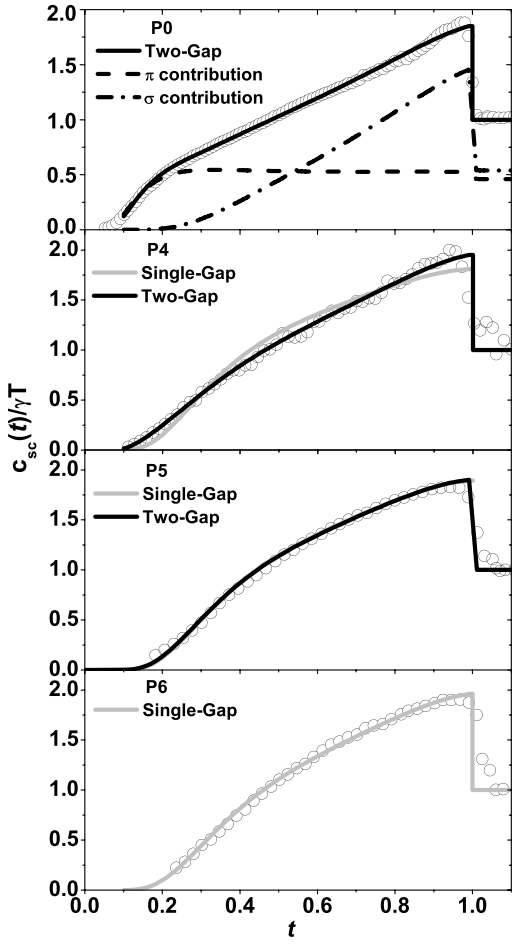

Fig. 3. Superconducting contribution of the specific heat as a function of reduced temperature for irradiated samples P0, P4, P5, P6. The gray lines represent the single-gap fit and the black lines are obtained by the two-gap fit. For the sample P0 the σ and π contributions at the specific heat are shown together with the two-gap fit.

specific heat at a reduced temperature of about 0.2 which cannot be taken into account by the σ-band contribution that, in this range of reduced temperature, has exponentially fallen down. Such excess is well evident in the less irradiated samples, but disappears in the most irradiated ones. In order to distinguish when the two gap superconductivity disappears, we systematically performed two fitting procedures: within a two-gap framework, three free parameters, α_σ, α_π and $x = \gamma_\sigma/\gamma$, were introduced whereas, within a single-gap framework, only one free parameter, $\alpha = \Delta(0)/k_B T_c$, was used.

For P0, P3.5 and P3.7, the experimental data can be reproduced only by considering two gaps. In the case of the sample P4, whose critical temperature is 21 K, both the two-gap that the single-gap best fit curves are displayed. It is clear that the single-gap curve (gray line) cannot reproduce the feature of the experimental data, and we conclude that for this sample the merging of the gaps has not occurred yet. The curves of P5 and P6, instead, can be fitted with the same accuracy by using single-gap and two-gap analyses. In these two samples, nearly equal values of χ^2 are obtained, despite the larger number of free parameters in the two-gap case. As shown in Fig. 3, for P5 ($T_c = 11$ K) the single and two-gap best fit curves perfectly overlap. In fact, the two-gap curve comes out to be the sum of nearly equal σ and π contributions; the so- obtained $\Delta_\sigma(0)$ and $\Delta_\pi(0)$ are very close each other and they coincide, within the errors, with $\Delta(0)$ obtained by the single-gap analysis. The same occurs for P6 ($T_c = 8.7$ K). For these samples there is no evidence of two separated gaps, and we conclude that the merging of the gap has occurred.

In Table 3 the best-fit parameters are reported together with the ones obtained with the same procedure on neutron irradiated polycrystalline sample by Wang et al. [18]. In this case, W0–W2 represent sample before irradiation (W0), after a subsequent dose of 10^{18} cm^{-2} (W1) and after a dose of 2×10^{18} cm^{-2} (W2). In Fig. 4, $\Delta_\sigma(0)$, $\Delta_\pi(0)$, and $\Delta(0)$ obtained in the two experiments are plotted as a function of T_c. We may easily distinguish two regions: for $T_c \geqslant 21$ K, the two-gap feature is observed, while for samples with $T_c < 20$ K, superconductivity is characterized by a single gap. In the two-gap region we find that $\Delta_\sigma(0)$

Table 3
The gap parameters estimated by the best fit procedure in Refs. [18,19]

Samples	T_c (K)	γ_σ/γ	$2\Delta_\sigma(0)/k_B T_c$	$2\Delta_\pi(0)/k_B T_c$
W0	37	0.5	3.9	1.3
W1	34.1	0.45	3.6	1.5
W2	30.2	0.45	3.6	1.7
P0	38.5	0.54 ± 0.05	3.8 ± 0.1	1.07 ± 0.06
P3.5	33.0	0.47 ± 0.03	3.7 ± 0.5	1.6 ± 0.2
P3.7	26.0	0.56 ± 0.05	3.5 ± 0.3	1.70 ± 0.1
P4	21.0	0.58 ± 0.08	3.5 ± 0.2	1.7 ± 0.1
P5	11.0		2.7 ± 0.1	
P6	8.7		2.8 ± 0.1	

$2\alpha_\sigma = 2\Delta_\sigma(0)/k_B T_c$, $2\alpha_\pi = 2\Delta_\pi(0)/k_B T_c$, and $x = \gamma_\sigma/\gamma$, evaluated for P0, P3.5, P3.7, P4; the best fit parameter $2\alpha = 2\Delta(0)/(k_B T_c)$ evaluated for P5, P6.

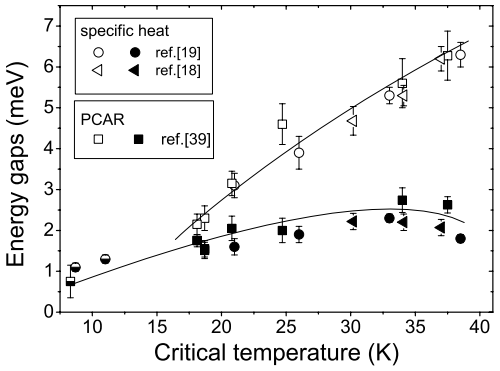

Fig. 4. $\Delta_\sigma(0)$ (empty symbols), $\Delta_\pi(0)$ (filled symbols) and $\Delta(0)$ (half-filled symbols) as a function of T_c from specific heat measurements (Refs. [18,19]) and PCAR spectroscopy (Ref. [40]). Gap amplitudes extracted from the fit of PCAR conductance curves are plotted as a function of the critical temperature of the junctions, T_c^A. Lines are only guides to the eye.

decreases almost linearly with T_c, while $\Delta_\pi(0)$ remains nearly constant. A close inspection shows that, out of the error bars, as T_c decreases, $\Delta_\pi(0)$ slightly rises, showing a flat maximum around 30–35 K, and then decreases.

In the single-gap region, not investigated before, $\Delta(0)$ decreases with T_c suppression, reaching a value of 1 meV at $T_c = 8.7$ K; the reduced gap values, $2\Delta(0)/k_B T_c$, are 2.8–2.7, lower than the BCS value 3.52. Reduced gap values lower than the BCS one were observed also in neutron irradiated V_3Si [33] and other a conventional disordered superconductor [34,35].

4.2. Point-contact Andreev-reflection (PCAR) spectroscopy

In its standard version, the point-contact (PC) technique consists in measuring the differential conductance curve (dI/dV vs. V) of a contact between a normal metal and the superconductor under study, made by gently pressing a sharp metallic tip against the sample surface. For best energy-resolved spectroscopy to be possible, the contact size a must be smaller than the mean free path in the superconductor, λ (ballistic regime). If the potential barrier at the interface is sufficiently small, the conduction through the contact is dominated by Andreev reflection, AR. This is a phenomenon in which an electron coming from the normal side is reflected back as a hole while a Cooper pair forms and propagates in the superconducting side [36]. The probability of AR is sensibly different from zero when the energy of the incoming electron is smaller than the gap in the superconductor [37]. The hallmark of AR is thus a doubling of the conductance when $|eV| < \Delta$ (in the ideal case of no potential barrier) or, more generally, an increase in conductance with symmetrical peaks at energies roughly corresponding to the gap edges. We actually used a modified, pressure-less version of the point-contact technique, in which the S–N junction is made by putting a small ($\varnothing \leqslant 50$ μm) drop of silver paint on the freshly cleaved surface of the sample. This technique ensures a good

mechanical stability of the contacts on thermal cycling and allows placing the contact in any point of the sample surface [38].

The contact characteristics can be tuned by means of short current or voltage pulses, which re-arrange the array of microscopic contacts between Ag particles and sample surface, until clear AR features are observed in the conductance curves. Some examples of these curves are reported, after normalization, in Fig. 5 for samples P0, P3.7, P4 and P6. Each panel also reports the value of the Andreev-critical temperature T_c^A, i.e. the temperature at which the Andreev-reflection features disappear and the normal-state conductance is recovered. Owing to the local nature of the PCAR measurements, T_c^A rather than the bulk T_c is the critical temperature to be compared to the gap(s) obtained in a given contact. To extract the gap values from the experimental curves, we fitted them with the Blonder–Tinkham–Klapwijk (BTK) model [37] generalised to the two-band case, i.e. we expressed the conductance G through the contact as the weighted sum of partial σ and π-band contributions: $G = w_\pi G_\pi + (1 - w_\pi) G_\sigma$. Each partial conductance contains three adjustable parameters: the gap amplitude Δ, the barrier parameter Z (that accounts for the potential barrier at the interface and the mismatch of Fermi velocities in the two banks) and a broadening parameter Γ that can be used, in this context, to account for intrinsic (lifetime) and extrinsic (experimental) sources of broadening. The weight w_π only depends on the direction of current injection with respect to the *ab* planes [39]. Owing to the non perfect directionality of PCAR [38] and to the polycrystalline nature of the samples, we always kept $w_\pi \sim 0.8$ [40]. The BTK curves that best fit the experimental data are shown in Fig. 5 as solid lines. In sample P0 the fit can only be obtained within the two-band BTK model. In samples P3.7, the two-band fit (black line) is preferable to the single-band one (grey line), which is unable to reproduce both the width of the Andreev-reflection structures and the position of the peaks. In sample P4, the single-band and the two-band BTK fit are almost equally good, and in fact the two lines are almost superimposed. In sample P6, the mean free path is so small that it was impossible to obtain contacts in the pure ballistic regime (contact size $a \ll \lambda$) so that the relevant curve shows small dips at about ±4 mV [41] that cannot be reproduced within the BTK model. Excluding these dips, the single-band model is sufficient to reproduce the position of the conductance peaks and the zero-bias dip between them. A two-band fit is possible, but gives two practically indistinguishable gaps.

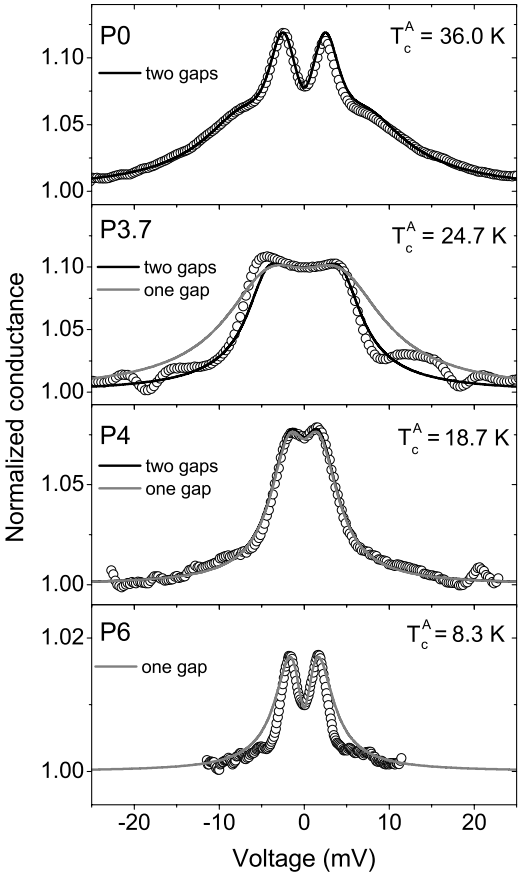

Fig. 5. Symbols: Experimental normalized conductance curves of various point contacts on samples P0, P3, P3.7, P4 and P6. Lines represent the best-fitting curves obtained within the single-band (gray) and two-band (black) BTK model. The values of the critical temperature of the contacts, T_c^A, are also indicated.

The gap values extracted from the fit of the conductance curves are reported as a function of T_c^A in Fig. 4, together with those obtained by specific-heat measurements. The results of the two-gap fit are shown in the region around 18–19 K, where the single-gap fit would give a gap $\Delta \approx \Delta_\pi$ that looks less compatible with the overall gap trend. The agreement between the two data sets is remarkable, despite the different techniques used. In the low-T_c^A region, the gap merging is unambiguously identified; the data trend suggests that it could occur at some T_c^A between 15 and 20 K. In the high-T_c^A region, the vales of Δ_π measured by PCAR are slightly greater than those measured by specific heat, as also observed in Al-doped MgB_2 [42], and a less marked increase in Δ_π is observed on decreasing T_c^A [40]. In any case, the trend of the data is perfectly consistent.

5. Scanning tunnelling spectroscopy on thin films

Scanning tunnelling spectroscopy (STS) is a powerful technique for locally measuring the superconducting gap, due to the dependence of the tunnel current on the local density of states (LDOS) of the sample surface. It actually provided the first unambiguous evidences of the existence of two gaps in MgB_2 [43–45]. In the frame of the present experiment, the broadening of the LDOS measured by STS can be analyzed in connection with scattering mechanisms induced by irradiation.

In a superconductor–insulator–normal metal (SIN) tunnel junction, the junction differential conductance at a given bias voltage V_0 is related to the superconducting DOS N_s by

$$\left.\frac{\mathrm{d}I}{\mathrm{d}V}\right|_{V_0} \propto |M|^2 \int \frac{N_s(E)}{N_{sn}(0)} \left.\frac{\mathrm{d}f(E-eV)}{\mathrm{d}(eV)}\right|_{V_0} \mathrm{d}E \quad (1)$$

In this formula, E is the quasi-particle energy, $E = 0$ representing the Fermi level, N_{sn} is the DOS of the superconducting electrode when it is in the normal state, f is the Fermi function evaluated at the measuring temperature T, M is the tunnel matrix element (approximatively considered energy independent).

At low temperatures, the smearing effect given by the derivative of f is minimized, and the tunnel differential conductance is very effective in directly testing the main features of the superconducting DOS such as the gap. Something more can be seen as concerns the particular case of the STS geometry and the MgB_2 samples.

In the scanning tunnelling microscope (STM) configuration, one of the electrodes (the normal one in our case) is a sharp conducting tip. This assures that only a very narrow region of the sample surface contributes to the tunnel current, allowing to probe the LDOS with high spatial resolution.

When measuring MgB_2, the following expression, developed for two band superconductors [2,46], can be used for the DOS in the π and σ bands:

$$\frac{N_{\sigma,\pi}(E)}{N_{\sigma,\pi}(0)} = \mathrm{Re}\left[\frac{u^2_{\sigma,\pi}(E)}{\sqrt{u^2_{\sigma,\pi}(E)-1}}\right] \quad (2)$$

The dimensionless functions u_σ and u_π are related each other by coupled equations involving the superconducting gaps Δ_σ and Δ_π, the intraband and interband scattering rates Γ_σ, Γ_π, $\Gamma_{\sigma\pi}$, $\Gamma_{\pi\sigma}$ [2,46]. The total measured tunnel DOS can be written as a linear combination of the two DOSs given by Eq. (2): $N^T(E) = \alpha_\sigma N_\sigma(E) + \alpha_\pi N_\pi(E)$, with $\alpha_\sigma + \alpha_\pi = 1$.

From the nature of $|M|^2$ [47], and due to the extremely narrow tunnel angle in the STM geometry, only quasi particles with momentum direction very close to the normal direction to the sample surface have a significantly non-zero tunnelling probability [44]. Therefore, differently from the other spectroscopic techniques, STS is strongly momentum-selective.

Since the STS experiments of this work were performed on c-axis oriented MgB_2 thin films, and due to the bidimensional nature of the σ Fermi surface with a low momentum dispersion along the c-axis [48], only quasiparticles from the π band contributed to the spectra that we measured. In such a case, it can be proved that the expression (2) leads to a simply BCS single-gap DOS, with gap and broadening given respectively by Δ_π and Γ_π. These circumstances strongly affected the nature of the measured STS spectra and their analysis.

Scanning tunneling spectroscopy (STS) experiments were performed at CNR-INFM/Coherentia in Naples on the films described in section III. The films were mounted on a scanning tunneling microscope (STM) in inert He atmosphere, with home-made PtIr tips. Reproducibility of tunnel spectra when changing the tunnel resistance assures a reduced role of contaminated surface layers.

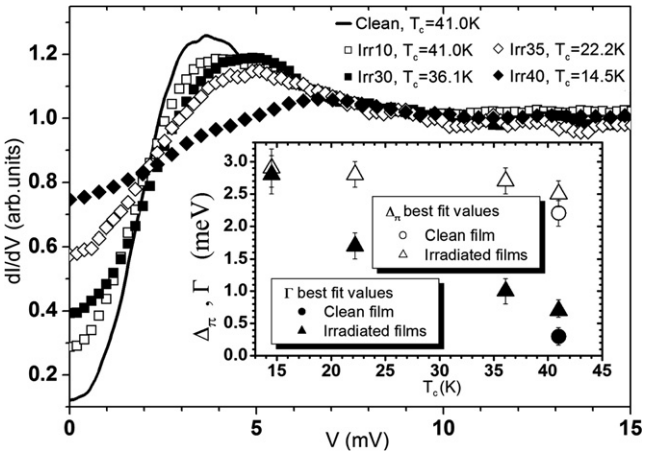

Fig. 6. STS spectra on MgB_2 thin films with different degree of irradiation. In the inset, the best fit values for Δ_π and Γ as a function of T_c.

Fig. 6 reports STS conductance spectra on differently irradiated samples. All the spectra were collected through a standard lock-in technique and were acquired (at $T = 4.2$ K) by stabilizing the feedback loop with a tunnel current of 100 pA and a bias voltage of 20 mV. A spectrum on a non irradiated film ($T_c = 41$ K, from Ref. [20]), measured in the same conditions, is also reported as a reference. Because of the c-axis orientation of the films, the π band contribution largely dominates and only one gap spectra were observed on all samples. As T_c decreases, with increasing neutron fluences, the zero-bias conductance increases and the coherence superconductivity peaks shift to higher voltages and appear less pronounced. Both effects reveal a broadening of the superconducting Local Density of States (LDOS) on the films as a consequence of the introduced disorder. Besides the smearing of LDOS, the shift of the peaks towards higher energies can be also due to an intrinsic change of the Δ_π value as disorder increases and T_c decreases. This can be proved by fitting the STS spectra through Eq. (1). According to what stated above, we used a BCS one-gap DOS with a broadening Dynes parameter Γ; the use of the complete two band model, with the estimated σ gap from the specific heat and point contact spectroscopy data on bulk samples irradiated through the same technique, does not change the extracted π gap value substantially, but introduces more free parameters, making the overall analysis less straightforward and clear.

The results of the fitting are shown in the inset of Fig. 6, where the estimated Δ_π and Γ values are plotted as a function of T_c. The plot reveals that Δ_π slightly increases with the degree of disorder, as predicted by the two-band model for increasing interband scattering [2,9]. In heavily irradiated thin films ($T_c = 22$ and 17 K), the extracted Δ_π values from the STS spectra are close to Δ_σ estimated in bulk samples (see Fig. 5) [45].

6. Discussion and conclusion

The results of three experiments described above can be briefly resumed as follows.

The specific heat and PCAR experiments have unambiguously stated that for T_c values above 18–20 K the two-gap feature remains evident, while below 11 K the single-gap superconductivity is completely established. Since the gaps are certainly still separated at 18–20 K, the merging has to take place at a temperature lower than the 25–20 K predicted for isotropic MgB_2. This result, with the lack of T_c saturation discussed above, suggests that disorder not only increases the interband scattering, but also affects the DOS [40]. On the other hand, the observation of single-gap superconductivity unambiguously indicates that interband scattering has effectively led to the merging of the gaps.

The STM experiment shows that Δ_π increases as T_c decreases and this is another clear evidence of the role of interband scattering. Moreover, in Ref. [45] it was shown that for T_c/T_{c0} ranging from 1 to 0.85 ($\Delta T_c = T_{c0} - T_c \approx 6$ K), Δ_π values extracted from STM and specific heat measurements increase in quantitative agreement with Δ_π predicted by the two-band model. For lower T_c, Δ_π is predicted to increase until the BCS value is reached at the saturation temperature, while experimental data remain below the theoretical curve. This suggests that for low levels of disorder the main mechanism of T_c reduction is the pair breaking due to interband scattering, while at higher levels of disorder other mechanisms cause the decreasing of Δ_π, and consequently the suppression of T_c.

Recently, the smearing of the DOS produced by disorder has been calculated for MgB_2, in analogy with A15 superconductors [49]. These results suggest that, at low level of disorder, the DOS is not affected by the smearing while at higher disorder the DOS, mainly of σ-band, reduces as an effect of intraband scattering processes. So, while at low level of disorder interband scattering is the leading mechanism that suppresses superconductivity and increases Δ_π, as far as the resistivity increases the DOS decreases suppressing the critical temperature and the energy gaps. In this framework, the isotropization should take place, but at a lower temperature than the predicted one [49].

In conclusion, we proved that neutron irradiation introduces disorder in a homogeneous and controlled way both in bulk and film materials. The overall experimental framework we presented is completely consistent and can be rationalized considering that disorder affects interband as well as intraband scattering processes.

Acknowledgements

This work is partially supported by MIUR through the project PRIN2006021741.

References

[1] J. Nagamatsu, N. Nakagawa, T. Muranaka, Y. Zenitani, J. Akimitsu, Nature 410 (2001) 63.
[2] H. Suhl, B.T. Matthias, L.R. Walker, Phys. Rev. Lett. 3 (1959) 552.
[3] P.B. Allen, B. Mitrovic, in: F. Seitz, D. Turnbull, H. Ehrenreich (Eds.), Solid State Physics, vol. 37, Academic, New York, 1982.
[4] A.A. Golubov, I.I. Mazin, Phys. Rev. B 55 (1997) 15146.
[5] I.I. Mazin, O.K. Andersen, O. Jepsen, O.V. Dolgov, J. Kortus, A.A. Golubov, A.B. Kuz'menko, D. van der Marel, Phys. Rev. Lett. 89 (2002) 107002.
[6] I.I. Mazin, V.P. Antropov, Physica C 385 (2003) 49.
[7] H.J. Choi, D. Roundy, H. Sun, M.L. Cohen, S.G. Louie, Phys. Rev. B 66 (2002) 020513.
[8] A.Y. Liu, I.I. Mazin, J. Kortus, Phys. Rev. Lett. 87 (2001) 087005.
[9] O.V. Dolgov, R.K. Kremer, J. Kortus, A.A. Golubov, S.V. Shulga, Phys. Rev. B 72 (2005) 024504.
[10] S.C. Erwin, I.I. Mazin, Phys. Rev.B 68 (2003) 132505.
[11] M. Putti, M. Affronte, P. Manfrinetti, A. Palenzona, Phys. Rev. B 68 (2003) 094514.
[12] M. Putti, C. Ferdeghini, M. Monni, I. Pallecchi, C. Tarantini, P. Manfrinetti, A. Palenzona, D. Daghero, R.S. Gonnelli, V.A. Stepanov, Phys. Rev. B 71 (2005) 144505.
[13] J. Karpinski, N.D. Zhigadlo, G. Schuck, S.M. Kazakov, B. Batlogg, K. Rogacki, R. Puzniak, J. Jun, E. Müller, P. Wägli, R. Gonnelli, D. Daghero, G.A. Ummarino, V.A. Stepanov, Phys. Rev. B 71 (2005) 174506.
[14] P. Samuely, Z. Holanova, P. Szabo, J. Kacmarcik, R.A. Ribeiro, S.L. Bud'ko, C. Petrovic, P.C. Canfield, Phys. Rev. B 68 (2003) 020205(R).
[15] H. Schmidt, K.E. Gray, D.G. Hinks, J.F. Zasadzinski, M. Avdeev, J.D. Jorgensen, J.C. Burley, Phys. Rev. B 68 (2003) 060508(R).
[16] R.S. Gonnelli, D. Daghero, A. Calzolari, G.A. Ummarino, V. Dellarocca, V.A. Stepanov, S.M. Kazakov, N. Zhigadlo, J. Karpinski, Phys. Rev. B 71 (2005) 060503(R).
[17] S. Tsuda, T. Yokoya, T. Kiss, T. Shimojima, S. Shin, T. Togashi, S. Watanabe, C. Zhang, C.T. Chen, S. Lee, H. Uchiyama, S. Tajima, N. Nakai, K. Machida, Phys. Rev. B 72 (2005) 064527.
[18] Y. Wang, F. Bouquet, I. Sheikin, P. Toulemonde, B. Revaz, M. Eisterer, H.W. Weber, J. Hinderer, A. Junod, J. Phys. Condens. Matter 15 (2003) 883.
[19] M. Putti, M. Affronte, C. Ferdeghini, P. Manfrinetti, C. Tarantini, E. Lehmann, Phys. Rev. Lett. 96 (2006) 077003.
[20] M. Iavarone, R. Di Capua, A.E. Koshelev, W.K. Kwok, F. Chiarella, R. Vaglio, W.N. Kang, E.M. Choi, H.J. Kim, S.I. Lee, A.V. Pogrebnyakov, X.X. Xi, Phys. Rev. B 71 (2005) 214502.
[21] A.E. Kar'kin, V.I. Voronin, T.V. D'yachkova, N.I. Kadyrova, A.P. Tyutyunik, V.G. Zubkov, Yu.G. Za nulin, M.V. Sadovski, B.N. Goshchitski, JETP Lett. 73 (2001) 570.
[22] M. Eisterer, M. Zehetmayer, S. Tonies, H.W. Weber, M. Kambara, N.H. Babu, D.A. Cardwell, L.R. Greenwood, Supercond. Sci. Technol. 15 (2002) L9.
[23] M. Zehetmayer, M. Eisterer, J. Jun, S.M. Kazakov, J. Karpinski, B. Birajdar, O. Eibl, H.M. Weber, Phys. Rev. B 69 (2004) 054510.
[24] M. Putti, V. Braccini, C. Ferdeghini, F. Gatti, G. Grasso, P. Manfrinetti, D. Marré, A. Palenzona, I. Pallecchi, C. Tarantini, I. Sheikin, H.U. Aebersold, E. Lehmann, Appl. Phys. Lett. 86 (2005) 112503.
[25] C. Tarantini, H.U. Aebersold, V. Braccini, G. Celentano, C. Ferdeghini, V. Ferrando, U. Gambardella, F. Gatti, E. Lehmann, P. Manfrinetti, D. Marré, A. Palenzona, I. Pallecchi, I. Sheikin, A.S. Siri, M. Putti, Phys. Rev. B 73 (2006) 134518.
[26] I. Pallecchi, C. Tarantini, H.U. Aebersold, V. Braccini, C. Fanciulli, C. Ferdeghini, F. Gatti, E. Lehmann, P. Manfrinetti, D. Marré, A. Palenzona, A.S. Siri, M. Vignolo, M. Putti, Phys. Rev. B 71 (2005) 212507.

[27] V. Ferrando, I. Pallecchi, C. Tarantini, D. Marré, M. Putti, F. Gatti, H.U. Aebersold, E. Lehmann, E. Haanappel, I. Sheikin, X.X. Xi, C. Ferdeghini. cond-mat/0608706. J. Appl. Phys., in press.
[28] R.T.H. Wilke, S.L. Bud'ko, P.C. Canfield, J. Farmer, S.T. Hannahs, Phys. Rev. B 73 (2006) 134512.
[29] A. Palenzona, P. Manfrinetti, V. Braccini, INFM Patent No. T02001A001098.
[30] X.H. Zeng, A.V. Pogrebnyakov, A. Kothcharov, J.E. Jones, X.X. Xi, E.M. Lysczek, J.M. Redwing, S. Xu, Qi Li, J. Lettieri, D.G. Schlom, W. Tian, X. Pan, Z.K. Liu, Nature Mater. 1 (2002) 35.
[31] J.M. Rowell, Supercon. Sci. Technol. 16 (2003) R17.
[32] F. Bouquet, Y. Wang, R.A. Fisher, D.G. Hinks, J.D. Jorgensen, A. Junod, N.E. Phillips, Europhys. Lett. 56 (2001) 856.
[33] R. Viswanathan, R. Caton, Phys. Rev. B 18 (1978) 15.
[34] K. Takanabe et al., Appl. Phys. Lett. 44 (1981) 559.
[35] C. Camerlingo, P. Scardi, C. Tosello, R. Vaglio, Phys. Rev. B 31 (1985) 3121.
[36] A.F. Andreev, Sov. Phys. JETP 19 (1964) 1228.
[37] G.E. Blonder, M. Tinkham, T.M. Klapwijk, Phys. Rev. B 25 (1982) 4515.
[38] R.S. Gonnelli, D. Daghero, G.A. Ummarino, V.A. Stepanov, J. Jun, S.M. Kazakov, J. Karpinski, Phys. Rev. Lett. 89 (2002) 247004.
[39] (a) A. Brinkman, A.A. Golubov, H. Rogalla, O.V. Dolgov, J. Kortus, Y. Kong, O. Jepsen, O.K. Andersen, Phys. Rev. B 65 (2002) 180517(R);
(b) A.A. Golubov, A. Brinkman, O.V. Dolgov, J. Kortus, O. Jepsen, Phys. Rev. B 66 (2002) 054524.
[40] D. Daghero, A. Calzolari, G.A. Ummarino, M. Tortello, R.S. Gonnelli, V.A. Stepanov, C. Tarantini, P. Manfrinetti, E. Lehmann, Phys. Rev. B 74 (2006) 174519.
[41] Goutam Sheet, S. Mukhopadhyay, P. Raychaudhuri, Phys. Rev. B 69 (2004) 134507.
[42] M. Putti, C. Ferdeghini, M. Monni, I. Pallecchi, C. Tarantini, P. Manfrinetti, A. Palenzona, D. Daghero, R.S. Gonnelli, V.A. Stepanov, Phys. Rev. B 71 (2005) 144505.
[43] F. Giubileo, D. Roditchev, W. Sacks, R. Lamy, D.X. Than, J. Klein, S. Miraglia, D. Fruchart, J. Marcus, P. Monod, Phys. Rev. Lett. 87 (2001) 177008.
[44] M. Iavarone, G. Karapetrov, A.E. Koshelev, W.K. Kwok, G.W. Crabtree, D.G. Hinks, W.N. Kang, E.M. Choi, H.J. Kim, S.I. Lee, Phys. Rev. Lett. 89 (2002) 187002.
[45] R. Di Capua, H.U. Aebersold, C. Ferdeghini, V. Ferrando, P. Orgiani, M. Putti, M. Salluzzo, R. Vaglio, X.X. Xi, Phys. Rev. B 75 (2007) 014515.
[46] N. Schopohl, K. Scharnberg, Solid State Commun. 22 (1977) 371.
[47] C.C. Sung, V.K. Wong, J. Phys. Chem. Solids 28 (1967) 1933.
[48] J. Kortus, I.I. Mazin, K.D. Belashchenko, V.P. Antropov, L.L. Boyer, Phys. Rev. Lett. 86 (2001) 4656.
[49] M. Putti, P. Brotto, M. Monni, E. Galleani, A. Sanna, S. Massidda, Europhys. Lett. 77 (2007) 57005.